

UC Davis

UC Davis Previously Published Works

Title

Frataxin deficiency increases cyclooxygenase 2 and prostaglandins in cell and animal models of Friedreich's ataxia

Permalink

<https://escholarship.org/uc/item/9nn019vc>

Journal

Human Molecular Genetics, 23(25)

ISSN

0964-6906

Authors

Hayashi, Genki

Shen, Yan

Pedersen, Theresa L

et al.

Publication Date

2014-12-20

DOI

10.1093/hmg/ddu407

Copyright Information

This work is made available under the terms of a Creative Commons Attribution License, available at <https://creativecommons.org/licenses/by/4.0/>

Peer reviewed

Frataxin deficiency increases cyclooxygenase 2 and prostaglandins in cell and animal models of Friedreich's ataxia

Genki Hayashi¹, Yan Shen¹, Theresa L. Pedersen³, John W. Newman^{2,3,4}, Mark Pook⁵
and Gino Cortopassi^{1,*}

¹Department of Molecular Biosciences and ²Department of Nutrition, University of California, Davis, CA 95616, USA, ³USDA, ARS, Western Human Nutrition Research Center, 430 West Health Sciences Dr, Davis, CA 95616, USA, ⁴West Coast Metabolomics Center, University of California Davis Genome Center, Davis, CA 95616, USA and ⁵Department of Biosciences, Brunel University, Uxbridge, Middlesex, UK

Received April 16, 2014; Revised July 2, 2014; Accepted August 4, 2014

An inherited deficiency of the mitochondrial protein frataxin causes Friedreich's ataxia (FRDA); the mechanism by which this deficiency triggers neuro- and cardio-degeneration is unclear. Microarrays of neural tissue of animal models of the disease showed decreases in antioxidant genes, and increases in inflammatory genes. Cyclooxygenase (COX)-derived oxylipins are important mediators of inflammation. We measured oxylipin levels using tandem mass spectrometry and ELISAs in multiple cell and animal models of FRDA. Mass spectrometry revealed increases in concentrations of prostaglandins, thromboxane B2, 15-HETE and 11-HETE in cerebellar samples of knockin knockout mice. One possible explanation for the elevated oxylipins is that frataxin deficiency results in increased COX activity. While constitutive COX1 was unchanged, inducible COX2 expression was elevated over 1.35-fold ($P < 0.05$) in two Friedreich's mouse models and Friedreich's lymphocytes. Consistent with higher COX2 expression, its activity was also increased by 58% over controls. COX2 expression is driven by multiple transcription factors, including activator protein 1 and cAMP response element-binding protein, both of which were elevated over 1.52-fold in cerebella. Taken together, the results support the hypothesis that reduced expression of frataxin leads to elevation of COX2-mediated oxylipin synthesis stimulated by increases in transcription factors that respond to increased reactive oxygen species. These findings support a neuroinflammatory mechanism in FRDA, which has both pathomechanistic and therapeutic implications.

INTRODUCTION

Friedreich's ataxia (FRDA) is the most common autosomal recessive ataxia affecting ~1:40 000 individuals (1). The disease is characterized by the neurodegeneration of dentate nucleus of the cerebellum and demyelination in spinocerebellar dorsal root ganglion neurons as well as hypertrophic cardiomyopathy and diabetes (2–4). Clinical symptoms of FRDA include gait ataxia affecting the motor coordination, weakness and atrophy of the extremities, and loss of lower-limb tendon reflexes. The disease is caused by reduced expression of frataxin gene attributed to the repeat expansion of GAA in the first intron of the gene or point mutation truncating the protein (1,5–7).

Extensive knowledge on the role of oxidative stress in the pathogenesis of FRDA exists including studies involving FRDA patient-derived cells and various mouse models. FRDA patient-derived cells have increased sensitivity to oxidative stress (8,9), and patients were observed to have increased markers of oxidative stress in their blood and urine (10–12). Furthermore, reduced Frataxin appears to reduce the level and or inducibility of Nuclear factor (erythroid-derived 2)-like 2 (NRF2) in cell and animal models of Friedreich's (13,14), which has been demonstrated to have anti-inflammatory effects in other systems patients may impair the induction of early antioxidant defenses resulting in increased cell lethality when under oxidative stress. Consistently, studies involving

*To whom correspondence should be addressed. Tel: +1 5307549665; Fax: +1 5303046810; Email: gcortopassi@ucdavis.edu

transgenic mouse models YG8 and YG22, both expressing human frataxin with trinucleotide repeat (GAA)^{≤190} reducing frataxin transcription showed signs of increased oxidative stress in the cerebellum, heart and skeletal muscles (14,15).

The prostaglandin (PG) pathway has been shown to be induced in response to oxidative stress and may be over stimulated by the chronic reactive oxygen species (ROS) elevation in frataxin-deficient models (16). PGs and thromboxanes are a subclass of eicosanoids produced by cyclooxygenase (COX)-mediated conversion of arachidonic acid in response to various stimuli (17–19). Previously we showed that inflammatory eicosanoids including PGs and thromboxane B2 (TXB2) and cytokines rose in frataxin-depleted Schwann cells (20). Consistent with the induction of inflammation in these frataxin-deficient cells, the decreased viability of the frataxin-deficient Schwann cells was rescued by known anti-inflammatory and anti-apoptotic drugs (20). Of the inhibitors, those targeting P38 kinases were most effective rescuers, suggesting a cAMP response element-binding protein (CREB) driven regulation of PG instigating the rescue in cell viability. Along with CREB, transcription factors, nuclear factor kappa-light-chain-enhancer of activated B cells (NFκB) and activator protein 1 (AP1) also regulate the expression of COX2 (21–23).

Inflammatory changes have been noted in the neurodegenerative conditions Alzheimer's disease (24,25), Parkinson's disease (26) and Amyotrophic lateral sclerosis (27,28). Given the previous implications of inflammatory PGs in cell models of FRDA pathogenesis, we investigated COX metabolites in cerebella of FRDA mouse models and patient B-lymphocytes. Significant differences were observed and an underlying mechanism is suggested.

RESULTS

Confirmation of frataxin deficiency in mouse and cell models by qRT–PCR

The cerebellar frataxin deficiency of the mouse frataxin knockin-knockout (KIKO) mouse was quantified by qRT–PCR; the animals contained 31% of frataxin compared with wild type (WT) mice as control ($P > 0.0032$, $n = 4$). Similarly, frataxin levels were quantified in the YG8 hemi and homozygote (15), and in cellular models of FRDA; all mutants were significantly deficient in frataxin. The hemizygote mice expressed 41% of frataxin as homozygote ($P > 0.00013$, $n = 4$) and patient-derived B-lymphocytes expressed 15.9% of frataxin compared with healthy B-lymphocytes ($P > 0.0021$, $n = 4$) (Fig 1).

Elevation of COX-derived oxylipins in frataxin-deficient mice

Oxylipins were measured in cerebella of frataxin knock-in/knockout (KIKO) deficient mice (29) using UPLC–MS/MS (Fig. 2). We quantified 33 arachidonic acid-derived oxylipins produced by COXs, lipoxygenases (LOXs) and cytochrome P450 (CYP). Twelve oxylipins were elevated in the KIKO mice ($P > 0.05$, $n = 4$) (Fig. 2), including the COX-derived prostanoids, thromboxanes, COX-side products 11 and 15 hydroxyeicosatetraenoic acids (HETE) (30), the CYP-derived

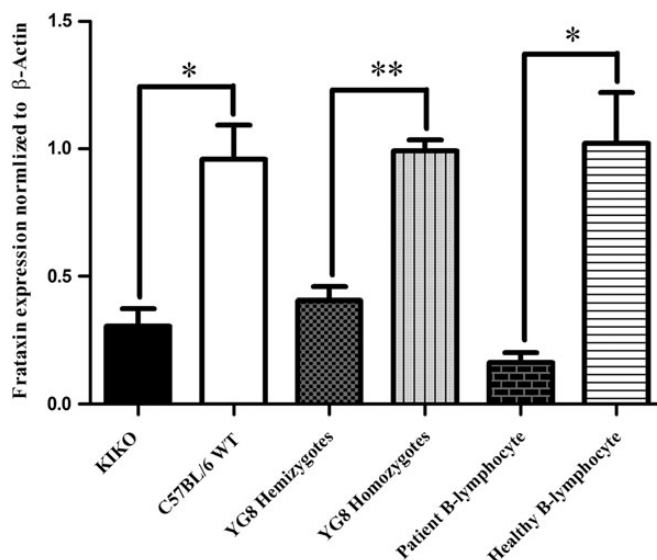


Figure 1. Reduced frataxin expression in frataxin-deficient models analyzed by qRT–PCR. Relative expression was normalized to β-actin and control using $\Delta\Delta C_T$ calculation. Cerebellum of KIKO showed 0.317-fold decreased expression compared with C57BL/6. Cerebellum of YG8 hemizygotes showed 0.410-fold decreased expression compared with YG8 homozygote. Patient B-lymphocytes showed 0.159-fold decreased expression compared with healthy B-lymphocytes. Bars represent averages \pm standard deviations ($n = 4$, $P < 0.005^*$, $P < 0.0005^{**}$).

epoxyeicosatrienoic acid (EET) and dihydroxyeicosatrienoic acid (DHET), and the 5LOX-derived HETE and keto-eicosatetraenoic acids (17,31,32). The results support the idea that frataxin deficiency in mice leads to increase in a global inflammatory response, including enhanced PG synthesis.

Frataxin-deficient animal and cell models have increased COX2 expression

To understand the source of prostanoid elevation, we measured the protein concentration of both COX1 and COX2, the constitutive and inducible COXs, respectively (17,19,33,34). For this experiment, we utilized three different models of frataxin deficiency. The first model as described previously is the cerebella of KIKO mouse model compared with WT control. The second model is the cerebella of YG8 mouse model knocked out for endogenous frataxin gene and inserted with mutant human frataxin transgene comparing hemizygote with a single copy of transgene expressing 41.0% that of homozygote (15).

COX 1 and 2 expression were also measured in human B-lymphocytes isolated from FRDA patients with 16.0% frataxin expression compared with healthy B-lymphocytes ($P > 0.0020$) (Fig. 1). Significantly increased protein levels of COX2 were observed in frataxin-deficient models, 4.16-fold in KIKO model ($P > 0.0030$, $n = 4$), 1.35-fold in YG8 model ($P > 0.039$, $n = 4$) and 1.92-fold in B-lymphocytes ($P > 0.019$, $n = 4$) while no changes in the expression levels of the constitutive isoform COX1 were detected (Fig. 3A–C).

Upstream of COX 1 and 2 is cytosolic phospholipase 2 (cPLA2), which hydrolyzes and releases arachidonic acid to be converted into PGG₂ by COX. Thus, cPLA2 can potentially alter the prostanoid profile (19,33). We measured the protein

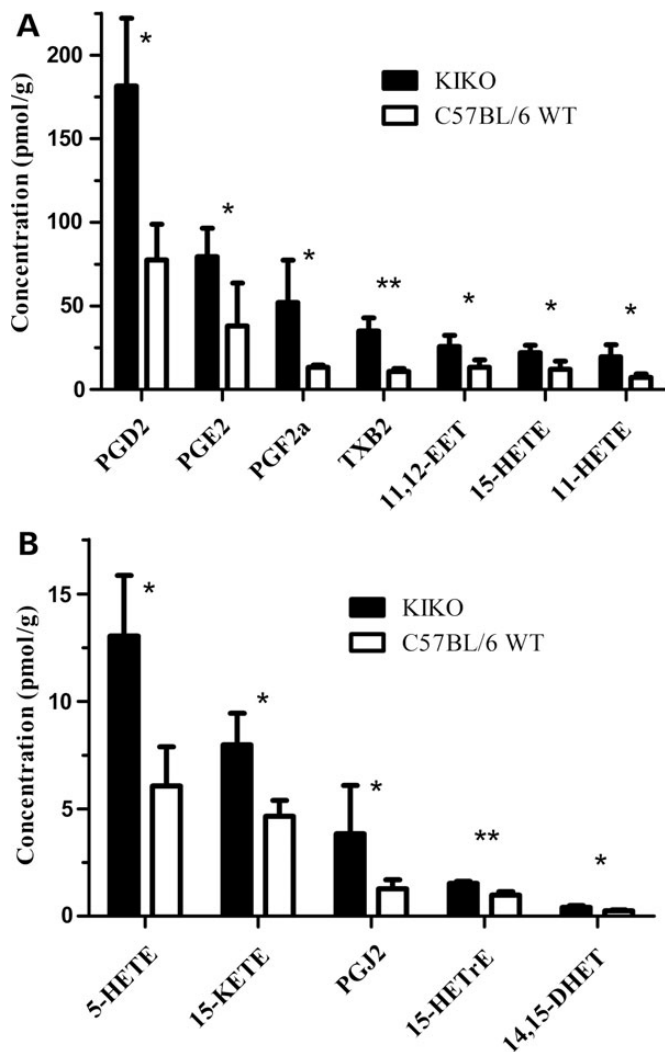


Figure 2. Inflammatory arachidonic metabolites are elevated in cerebellum of frataxin-deficient KIKO mouse model. (A and B) 12 arachidonic metabolites converted by COX, lipoxygenase and cytochrome P450 were identified to be significantly increased. Grubbs test was used to exclude outliers assuming normal distribution. Bars represent averages \pm standard deviations ($n = 4$, $P < 0.05^*$, $P < 0.005^{**}$).

level of both cPLA2 and its active form, phosphorylated at serine 505, and detected no significant difference between KIKO and WT mouse cerebellum ($n = 4$) (Fig. 3D). Taken together, these results support the notion that increased COX2 expression, rather than COX1 or cPLA2 activity, is the cause of increased prostanoid levels in frataxin-deficient models.

Increased COX activity in frataxin-deficient mice and cells

In order for an increase of COX expression to impact prostanoid concentrations, the increase must impact COX activity. Thus we analyzed the arachidonate metabolites of the KIKO cerebellar tissue normalized to both total concentration of unbound arachidonic acid and also to WT to identify the relative activity of downstream enzymes. In mutants the COX metabolites were 3.05-fold higher than WT, 15LOX metabolites were 1.94-fold higher than WT, 5LOX metabolites were 2.24-fold higher than

WT, CYP metabolites were 1.33-fold higher than WT, and other arachidonic acid metabolites were 1.20-fold higher than WT ($n = 4$) (Fig. 4). COX metabolites were significantly higher than those of 15LOX ($P > 0.02$), CYP ($P > 1.54 \times 10^{-5}$) and other arachidonate metabolites ($P > 1.13 \times 10^{-6}$). We also observed significant elevation of 5LOX metabolites compared with CYP ($P > 0.03$) and other arachidonate metabolites ($P > 0.018$) ($n = 4$) (Fig. 4).

We also performed an ELISA-based activity assay measuring the conversion rate of hydrolyzed arachidonic acid to PGG₂, a precursor to PGH₂. Comparing the cerebellum of frataxin-deficient mouse KIKO and YG8, and patient B-lymphocyte to either WT or healthy controls, we found significant elevation of COX activity when normalized to indomethacin-inhibited samples. KIKO hemizygote showed 1.58-fold activity ($P > 0.030$, $n = 3$), YG8 hemizygote showed 2.21-fold activity ($P > 0.0012$, $n = 4$) and patient B-lymphocyte showed 1.92-fold activity ($P > 0.0069$, $n = 4$) relative to their respective controls (Fig. 5). Taken together with the immunoblot results, the likely driving force of increased prostanoid concentration in the frataxin-deficient models is the overexpression and the subsequent increased activity of COX2.

Elevated CREB and AP1 transcription factors explain COX2 overexpression in frataxin-deficient cells

Expression of the COX2 gene is driven by multiple positive factors, including NF κ B, CREB and AP1. To understand whether or how frataxin deficiency was driving an intrinsic increase in COX2 gene activity, we used antibody specific to activated transcription factors, phosphorylated NF κ B (ser536), phosphorylated CREB (ser133) and phosphorylated AP1 (ser63) known to positively regulate COX2 expression, in the cerebella of KIKO mouse (21–23). We found no difference in the activation of NF κ B ($n = 6$) but identified a 3.67-fold increase in CREB activation ($P > 0.0024$, $n = 6$) and 1.52-fold increase in AP1 activation ($P > 0.028$, $n = 6$) (Fig. 6A and B). This suggests that in the context of the frataxin-deficient cerebellum, CREB and AP1 increase drive the COX2 overexpression and increased PG production.

Increased microglial activation in lipopolysaccharide induced frataxin-deficient mouse cerebellum

To understand whether COX2 overexpression and increased prostanoids were having an impact on neuroinflammation in the frataxin-deficient context, we measured ionized calcium-binding adapter molecule 1 (Iba1), a known marker of microglial neuroinflammation in the cerebella of YG8 mice, in the context of the experimental inflammogen lipopolysaccharide (LPS) (20,35). The treatment of WT with LPS did not significantly increase the expression of Iba1 in cerebellum with 1.16-fold elevation, but the same treatment in the YG8 hemizygotes had significantly increased the Iba1 expression by 1.37-fold ($P > 0.0096$, $n = 4$). Accounting for baseline Iba1 expression in WT and YG8 hemizygote cerebellum treated with PBS, YG8 hemizygotes had 17% increase in induction of Iba1 by LPS compared with WT (Fig. 7A and B). Thus, frataxin deficiency increased the reactivity of Iba1 staining microglia in the context of LPS treatment relative to WT.

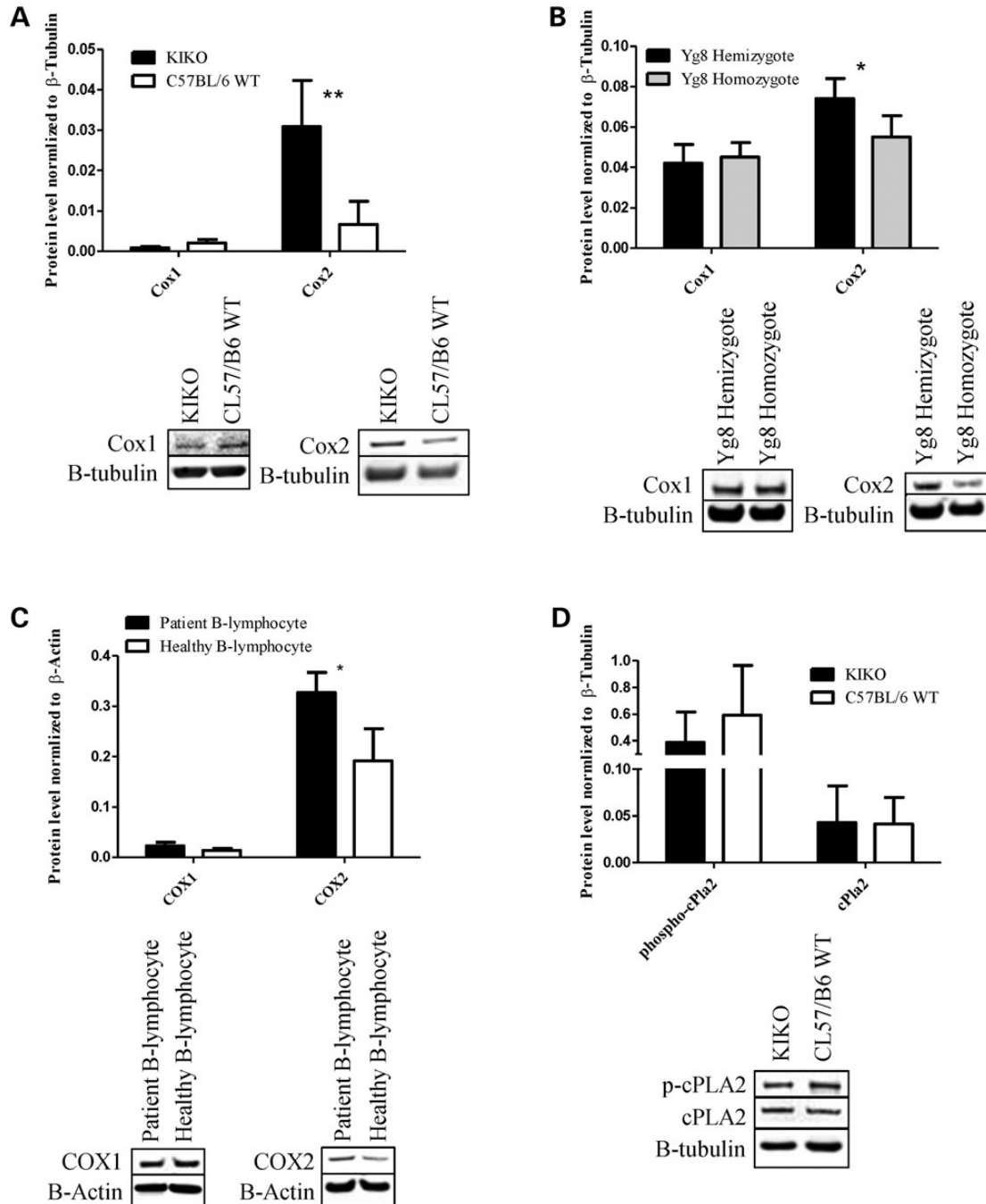


Figure 3. Frataxin-deficient models have increased expression of COX2 and no alterations in COX1 or cPLA2 expression. (A and D) Cerebellum of KIKO has 4.40-fold increased expression of Cox2 while no changes in Cox1 and cPLA2 or the active phosphorylated cPLA2 were observed compared with C57BL/6 WT. (B) Cerebellum of YG8 hemizygote showed 1.35-fold increased Cox2 expression and no change in Cox1 expression was observed compared with YG8 homozygote. (C) Patient B-lymphocytes had 1.71-fold increased expression of COX2 expression with no changes in COX1 expression compared with healthy B-lymphocytes. The KIKO and YG8 samples were normalized to β -tubulin and B-lymphocyte samples were normalized to β -actin. Bars represent averages \pm standard deviations ($n = 4$, $P < 0.05^*$, $P < 0.005^{**}$).

DISCUSSION

FRDA is an autosomal recessive disease characterized by the degeneration of the dorsal root ganglion and cerebellum (2,4).

Clinical symptoms of FRDA include gait ataxia affecting the motor coordination, weakness and atrophy of the extremities, and loss of lower-limb tendon reflexes (5,36,37). The disease state is caused by the reduced expression of a nuclear encoded

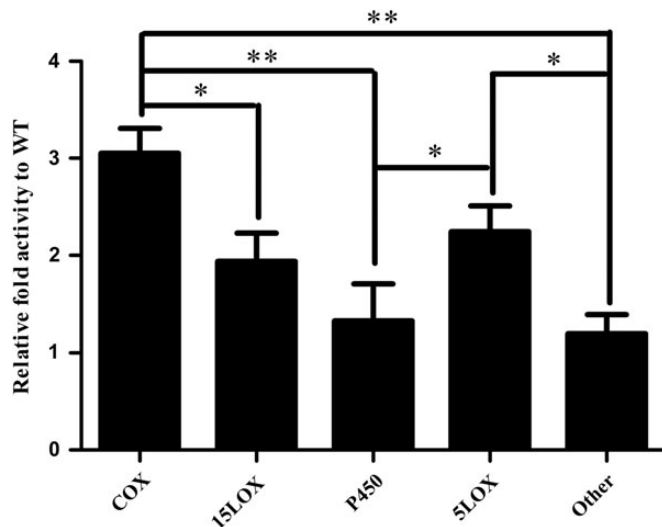


Figure 4. Frataxin-deficient KIKO mice have elevated COX metabolites normalized to free arachidonic acid relative to WT. All oxylipids downstream of arachidonic acid were normalized to total concentration of unbound arachidonic acid and fold change calculated relative to WT for the same metabolite. The COX metabolite (TXB₂, PGF_{1a}, PGE₂, PGD₂, PGJ₂, PGF_{2a} and 11 HETE) was 3.05-fold higher than WT, 15LOX metabolite (15 HETE) was 1.94-fold higher than WT, 5LOX metabolite (5 HETE) was 2.24-fold higher than WT, CYP metabolism (14,15DHET and 11,12-DHET) was 1.33-fold higher than WT, other arachidonate metabolism (8,15DHET, 5,15DHET, 9HETE and 8HETE) was 1.20-fold higher than WT. Bars represent averages \pm standard error mean ($n = 4$, $P < 0.05^*$, $P < 0.0005^{**}$).

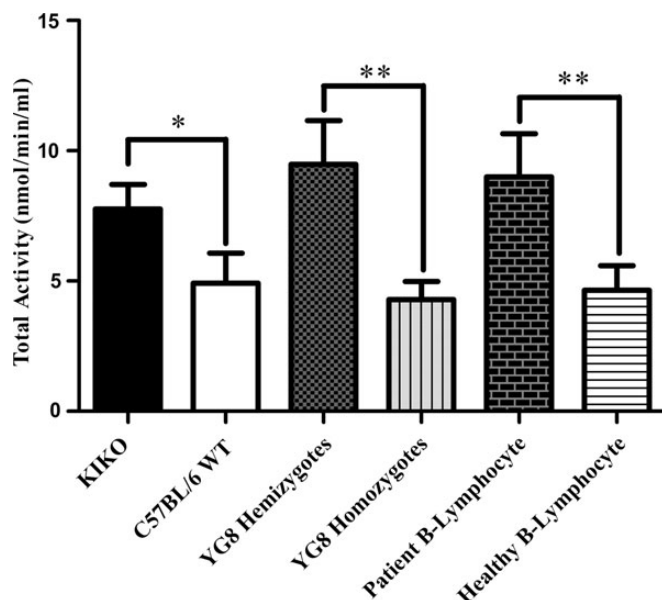


Figure 5. Frataxin-deficient models have increased total COX activity of cerebellar or B-lymphocyte lysate. All FRDA models, KIKO, YG8 and patient B-lymphocytes showed 1.58-, 2.21- and 1.94-fold increase in COX activity respectively to each model's control. Bars represent averages \pm standard deviations ($n = 3-4$, $P < 0.05^*$, $P < 0.01^{**}$).

gene, frataxin mediated by the repeat expansion of GAA within the first intron of the gene altering the epigenetic control of the gene transcription (6,7,38). However, the pathomechanism by

which frataxin deficiency causes neuro- and cardio-degeneration is not clear. We previously demonstrated inflammatory consequences of frataxin knockdown in Schwann tissue culture cells (20), and also induction of inflammatory transcripts and suppression of antioxidant and NRF2 anti-inflammatory molecules in a mouse model of FRDA (14). The reduced capacity of NRF2 and thiol antioxidant proteins (Glxr1, Gstm1 and Prdx3) is thought to be involved in the production of ROS in the cerebellar tissue and possibly in the lymphocyte cells by suppressing the cell's capacity to maintain homeostatic anti-oxidative capability. The suppression of the anti-inflammatory factor NRF2, and the elevated expression of the pro-inflammatory prostaglandin D₂ synthase (PTGDS) transcript motivated a search for changes in inflammatory mediators in brains of a Friedreich's animal model.

Four PGs and TXB₂ were elevated significantly in KIKO mice over controls. Of the elevated eicosanoids, 8 of 12 were the products of COX-mediated conversion of arachidonic acid, supporting the notion that the COX activity could play a role (Fig. 2A and B) (17,31,32). We also observed elevation of LOX and CYP metabolized products, which have been previously reported and may be the result of parallel pathway activated by oxidative stress (24,26,28,39). Many of the non-COX metabolite mass spectrometry hits including 11,12EET, 15HETRe and 5HETE have been reported to have anti-inflammatory effects in response to excess production of ROS (40–42). Interestingly, 15LOX and COX mediated metabolite 15HETE is believed to be involved in the progression of Alzheimer's disease and the reduction of 15HETE in Alzheimer's model shows evidence of decreased oxidative stress (32,43). Furthermore, increase of specific CYPs may also contribute to the compounding problem of oxidative stress by synthesizing ROS but this effect has yet to be investigated in the context of FRDA (44). Similar rises in prostanoid synthesis have been reported to have neuroinflammatory effects leading to neurodegeneration (45). PGs including PGE₂ and 15d-PGJ₂ have been associated with pathogenesis of neurodegenerative diseases such as Alzheimer's disease (24,25), Parkinson's disease (26) and Amyotrophic lateral sclerosis (27,28).

We also looked into more general lipid composition analysis to determine whether frataxin deficiency simply elevates lipid synthesis nonspecifically. Mass spectrometry analysis revealed only minor elevation of total fatty acid in the KIKO mice compared with those of WT, but the major elevation was observed in the COX-mediated oxylipid metabolism, supported by slight decrease in the concentration of linoleic acid (C18:2n6) in the KIKO mice (Supplementary Material, Fig. S1). The frataxin-deficient KIKO mouse has increased concentration of prostanoids synthesized primarily by COX, and this elevation may contribute to increased inflammation, which may ultimately lead to degeneration of the dorsal root ganglion and cerebellum.

The action of both COX and cPLA₂ play key roles in the synthesis of prostanoids. Initially, cPLA₂ regulates the availability of free arachidonic acid by hydrolysis and cleavage from the phospholipid bilayer followed by COX-mediated conversion of arachidonic acid to the prostanoids (17–19,27,46). In this study we showed by immunoblot analysis of KIKO and YG8 cerebellum as well as B-lymphocyte cells, the likely cause of prostanoid concentration elevation observed by mass spectrometry (Fig. 2A and B) resulted from the overexpression of the inducible COX isoform, COX2 rather than the constitutive isoform, COX1 (19,33,34) (Fig. 3A–C). We identified no

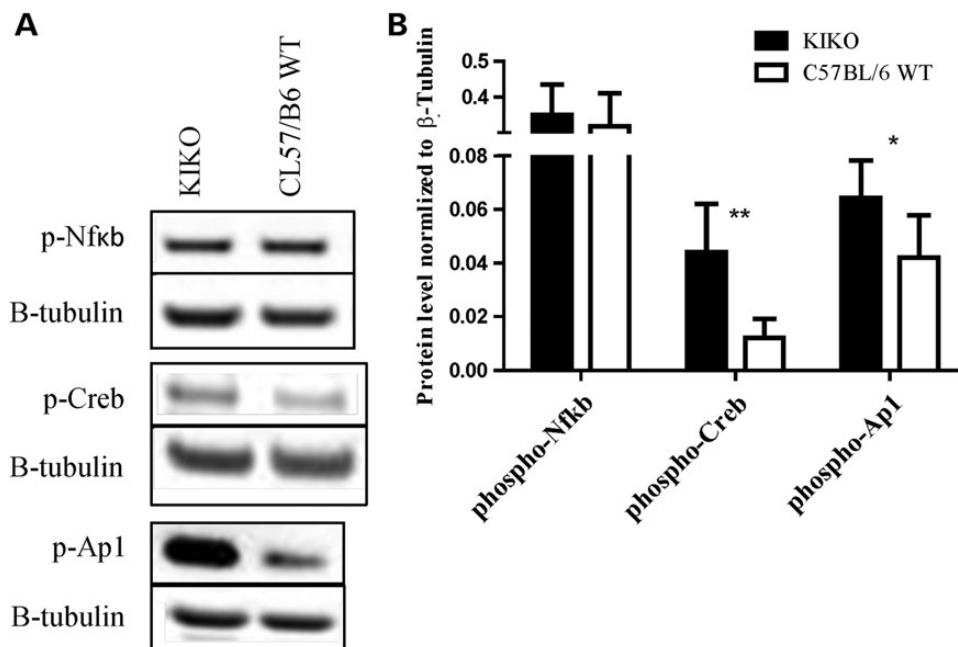


Figure 6. Cerebellum of frataxin-deficient KIKO mouse model has increased activation of transcription factors CREB and AP1. (A and B) KIKO shows 3.67- and 1.52-fold increase of CREB and AP1 activation, respectively. Activation is marked by phosphorylation. Bars represent averages \pm standard deviations ($n = 6$, $P < 0.05^*$, $P < 0.005^{**}$).

alterations in protein concentration of cPLA and phospho-cPLA in the KIKO mice, indicating that cPLA2 does not cause the increased prostanoid burden in mutant mice (Fig. 3D) (46).

Total COX activity assays also supported the notion that COX2 overexpression has increased the conversion rate of arachidonic acid to downstream prostanoids (Fig. 5). These data are supported by arachidonate metabolite analysis, indicating that the more of the unbound arachidonic acid is being converted into downstream metabolites of COX than any other enzyme (Fig. 4). Both 15- and 5-LOX activity appear to be elevated compared with WT, which may be a consequence of basally elevated ROS in the frataxin-deficient state (32,42). Taken together, the reduction in frataxin expression has increased the expression of COX2 increasing the synthesis of prostanoids. Given the increased prostanoid profile in the KIKO mouse model, one could consider the reversal of COX2 overexpression by NSAIDs, but this was beyond the scope of this work, but is a future prospect.

COX2 expression is regulated by three transcription factors, NF κ B, CREB and AP1, and of these, we have found increased activation of CREB and AP1 (22). The CREB and AP1 activation was 3.67 and 1.52-fold higher in the KIKO mice, respectively, indicating multiple pathway activation of COX2 transcription and the greater role of CREB in COX2 activation (Fig. 6A and B). Both CREB and AP1 transcription factors have been reported to be activated by cytokine pathways mediated through the presence of ROS (23,47). Interestingly, the chronic elevation of oxidative stress in FRDA patients and animal models may be a contributing factor in the activation of cytokines responsible for COX2 overexpression (8–12), suggesting the mechanism fxn-deficiency \rightarrow ROS \rightarrow cytokines \rightarrow CREB/AP1 \rightarrow COX2 \rightarrow iba1/microglial activation \rightarrow neuroinflammation \rightarrow neurodegeneration (Fig. 8). It cannot be ruled out that the dysregulation of NRF2 in the

frataxin-deficient mice (14) (Supplementary Material, Fig. S3) is uninvolved in the overexpression of COX2 as it has previously been shown to be the case in the brain of Nrf2 $^{-/-}$ mice and plays a role in further elevating inflammatory state of frataxin-deficient mice (48).

One question that arises from these data in Friedreich's patient cells and two mouse models is whether evidence of inflammation is also observed in either living Friedreich's patients or autaptic tissue. There is clear evidence of inflammation in Friedreich's autaptic hearts marked by cluster of differentiation 68 (CD68) positive cells (49); CD68 is a marker of microglial activation. Microglia are more activated in brains of LPS-stimulated mutant mice than in controls, consistent with a frataxin-dependent increase in microglial activation in these cerebellar samples (Fig. 7). These data suggest that frataxin deficiency leads to microglial activation in Friedreich's hearts and mouse model brains. We see increased production of oxylipins in cerebella of mutant mice, and the median increase was mild, about 56% (Supplementary Material, Fig. S2). These mice also have a mild neurobehavioral phenotype, and a mild amount of neurodegeneration. Similarly, we do not see a difference in iba1-positive microglia at baseline; the effect is once again mild and is only visible and significant when provoked with an experimental inflammogen (LPS). Thus, either as a cause or effect of the mild rise in oxylipins, there is more 'inducibility of inflammation' in the mutant mice. Furthermore, active microglia has been shown to produce ROS, mainly nitrogen oxide further exacerbating the problem (44). Telomere length, an indirect marker of inflammation, was also measured in Friedreich's patient plasma correlating disease duration with reduction in telomere lengths (50–52). These cases represent the need for further research concerning inflammation as a possible pathomechanism of FRDA.

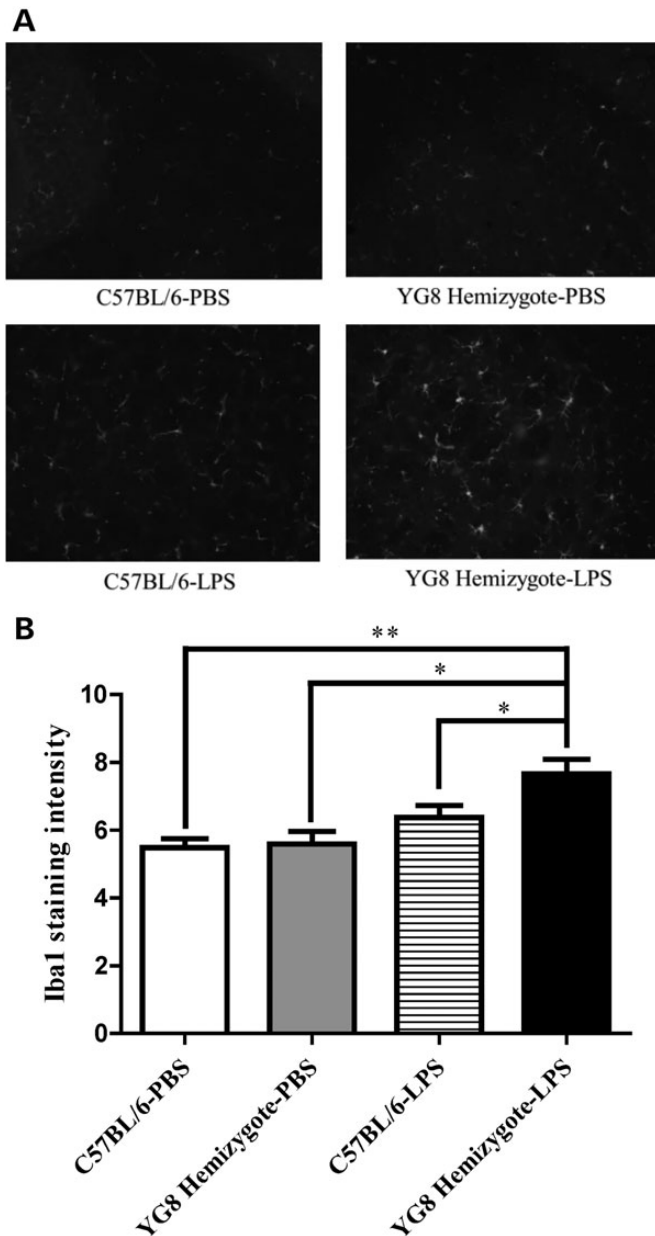


Figure 7. Frataxin-deficient YG8 hemizygote mouse cerebellum shows increased inducibility of inflammation with LPS treatment compared with WT. (A) Immunohistochemistry of frataxin-deficient YG8 hemizygote and WT cerebellar section with antibody specific to Iba1. The LPS treatment has increased the protein concentration of Iba1 in mutants 1.37-fold compared with WT which increased 1.16-fold from similar baseline expression in the PBS treatment. (B) Quantification of immunohistochemistry. Bars represent averages \pm standard deviations ($n = 4$, $P < 0.05^*$, $P < 0.005^{**}$).

In conclusion, we have shown in cerebellum of frataxin-deficient mouse models KIKO and YG8, and patient derived lymphocytes, that frataxin deficiency leads to increased activation of transcription factors CREB and AP1 mediating the over-expression of COX2 subsequently elevating concentrations of multiple prostanoids, and that cerebella of such mice are more sensitive to a neuroinflammatory stimulus (Fig. 7). Further studies are necessary to understand the extent to which

neurodegeneration of dorsal root ganglion and cerebellum in FRDA is caused by prostanoid alteration, and if the causal regulatory changes are due to chronic elevation of ROS. If prostanoid synthesis is involved in the pathogenesis of FRDA, anti-inflammatory treatments targeting COX, or upstream transcription factors CREB and AP1 may open new avenues for FRDA treatment.

MATERIAL AND METHODS

Cell culture

Human B-lymphocyte cells; GM16220, GM16197, GM15851, GM15850, GM04079, GM00607, GM00333 and GM00130 (Coriell Institute) were maintained at 37°C in humidified atmosphere with 5% CO₂. DMEM (Cellgro) supplemented with 15% fetal bovine serum (JR-Scientific), 2 mM sodium pyruvate (Sigma-Aldrich), 1 \times antibiotic-antimycotic, 1 \times MEM non-essential amino acids (Gibco), and 50 mg/ml uridine (MP-Biomedicals) was used to grow cells.

Mouse models and dissection

Human transgenic frataxin-deficient mice YG8 (15) (YG8Pook/J; Jackson Laboratory, Sacramento, CA, USA) and endogenous frataxin-deficient KIKO mice [a kind gift from Dr. Pandolfo (29)] were housed in a vivarium maintained at 22–24°C and 40–60% relative humidity with a 12-h light/12-h dark cycle. All experimental procedures were approved by the University of California Institutional Animal Care and Use Committee.

The mice were decapitated and cerebellums were immediately removed and then flash frozen with liquid nitrogen. Samples were stored in -80°C until utilized for mass spectrometry, quantitative PCR, western blot and COX activity assay.

RNA extraction and quantitative RT-PCR

Total RNA was extracted from cerebellar tissue of frataxin-deficient KIKO and YG8 mice as well as B-lymphocyte cells using RNeasy plus mini kit (Qiagen) following manufacturer's instruction and RNA quantity measured by NanoDrop 2000c Spectrophotometer (Thermo Scientific).

Quantitative PCR was performed using the Superscript III One Step kit (Invitrogen) per manufacturer's instruction in a Roche Lightcycler 480 (Roche Diagnostics). Primer sequences are β -actin Forward GCCAACACAGTGCTGTCTGG, β -actin Reverse CTGCTTGCTGATCCACATCTGC, YG8 FXN Forward CTGGCTATCTTCTCCATCCAG, YG8 FXN Reverse AGCA TCTTTTCCGGAATAGGC, KIKO Fxn Forward GATCAA CAAGCAGACCCCAAA, KIKO Fxn Reverse AGGCCAATG AAGACAAGTCCA, B-Lymphocyte FXN Forward ATCTT CTCCATCCAGTGGACCT and B-Lymphocyte FXN Reverse GCTGGGCATCAAGCATCTTTT. The data were analyzed by delta delta CT method.

Protein extraction and western blot analysis

Mouse cerebellar tissues and B-lymphocyte cell pellets were homogenized with a cell lysis buffer (Cell Signaling) with Halt phosphatase inhibitor (Thermo-Fisher), complete protease

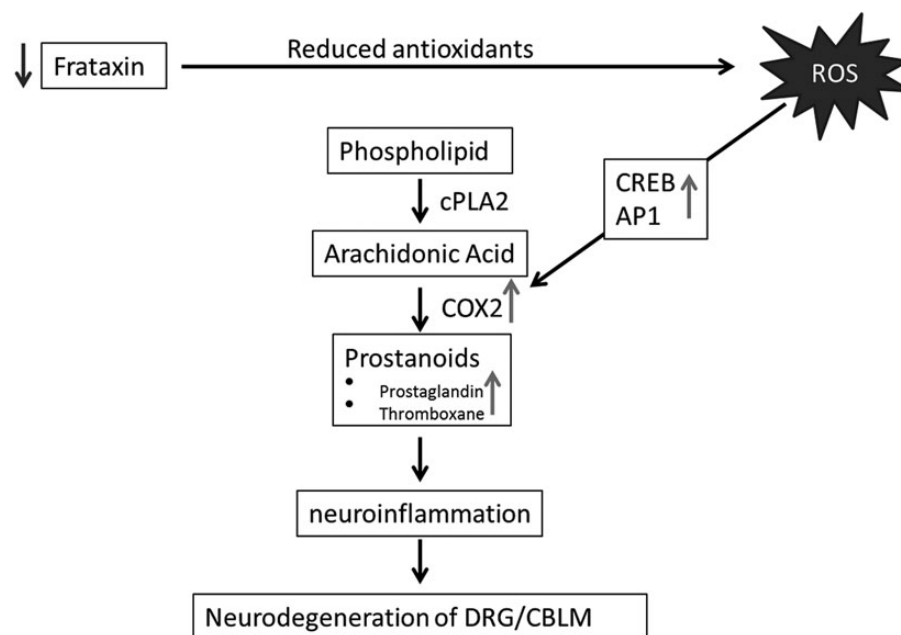


Figure 8. Model for frataxin deficiency with elevation of prostanoids leading to neurodegeneration of dorsal root ganglion (DRG) and cerebellum (CBLM).

inhibitors (Roche) and PSMF (Sigma-Aldrich). Thirty micrograms of lysates were loaded into 4–12% Bis–Tris gels (Invitrogen). Electrophoresis was carried out according to the manufacturer's recommendations. Following electrophoresis, the proteins were transferred to nitrocellulose membranes by the iBlot device (Invitrogen), blocked with an Odyssey blocking buffer (LI-COR Biotechnology) for 1 h. Membranes were incubated overnight with the following primary antibodies in blocking buffer: COX1 (ab133319 for human, ab133319 for mouse; Abcam), COX2 (ab62331 for human, ab6665 for mouse; Abcam), phospho-CREB (4095), phospho-cJun/AP1 (5464), phospho-NF κ B (4025; Cell signaling), cPLA2 (sc-454), phospho-cPLA2 (sc-34391; Santa Cruz Biotech, Santa Cruz, CA, USA), β -actin (A5441; Sigma-Aldrich), and β -tubulin (DSHB-E7; DSHB, Iowa). Subsequently, the membranes were incubated with a corresponding pair of IRDye 680CW and IRDye 800CW-coupled secondary antibodies (LI-COR). Proteins were visualized with the Odyssey infrared imager and software (LI-COR) according to the manufacturer's instruction.

LPS administration and immunostaining of Iba1

Female YG8 mice or C57BL/6 mice were intraperitoneally injected with a single dose of LPS (5 mg/kg). Mice were perfused with 4% paraformaldehyde in 0.1 M PBS at 24 h after LPS injection. The animals were anesthetized and then perfused with 4% paraformaldehyde in 0.1 M PBS (pH 7.4) and cryoprotected in 30% sucrose in 0.1 M PBS. 15 μ m coronal brain sections from cerebellum were cut by cryostat. Representative sections were stained with Iba1 antibody (1:100; Wako, VA, USA) followed by a fluorescent secondary antibody (Invitrogen, NY, USA). The images of Iba1 fluorescent immunostaining were taken with Nikon camera (Tokyo, Japan). Fluorescent intensity from six fields of each animal was measured by Image J software.

COX activity

Total COX activity was measured with COX Fluorescent Activity Assay Kit (Cayman Chemical, Ann Arbor, MI, USA) according to manufacturer's instruction normalized to samples incubated with Indomethacin (Sigma-Aldrich).

Tissue extraction

Frozen mouse cerebellar samples (20–100 mg) were pulverized on dry ice, after mixing with 5 μ l BHT/EDTA (0.2 mg/ml in 1:1 methanol/water), and 30 μ l methanolic surrogate solutions containing a suite of labeled surrogates to quantify cholesteryl ester, triglyceride, phospholipid, free fatty acid, prostanoid, thromboid, diol, alcohol, epoxide and sphingoid bases. Samples were introduced to two pre-cleaned stainless steel balls and vortexed with 500 μ l methanol for 3 min. Samples were pelleted by centrifugation for 5 min at 10 000 rcf, 10°C, and the supernatant was isolated. Residues were mixed with 350 μ l 2-propanol, homogenized and pelleted and the supernatant was combined with the primary methanolic extract. The residue was extracted a third time with 350 μ l cyclohexane, followed by mixing and supernatant isolation and combination with the other organic isolates. Solvents were removed by vacuum evaporation for 60 min without heating and reconstituted in 100 μ l toluene and mixed with 100 μ l methanol. A 10 μ l aliquot of the extract was isolated for fatty acid analyses while 180 μ l were evaporated to dryness and reconstituted in 100 μ l methanol containing 1-cyclohexyl-3-ureido-dodecanoic acid (CUDA), filtered at with Amicon® Ultrafree-MC Durapore PVDF 0.1 μ m filters (Millipore, Billerica, MA, USA) and used for the quantification of oxylipins.

UPLC-tandem mass spectrometry

Analytes were separated by reverse phase ultra-performance liquid chromatograph with a 1.7 μ m Acquity BEH column

(Waters, Milford, MA, USA) using a 16 min gradient (Solvent A = 0.1% acetic acid; Solvent B = 90:10 v/v acetonitrile/isopropanol), detected on an API 4000 QTrap (AB Sciex, Framingham, MA, USA) by multiple reaction monitoring after negative mode electrospray ionization, and quantified against 6 point calibration curves using internal standard methodologies as previously reported (doi:10.1371/journal.pone.0089393). Data reporting criteria include: data >3:1 signal to noise; the relative contribution of background from method blanks is <25% of signal; values are within the calibrated linear range.

Data analysis

Quantified results were manually curated to confirm accurate integrations. NEFA results for a single sample (ID#1) were statistical outliers by the Dixon's Q-test and were excluded. All missing values were computationally imputed using a probabilistic principal components analysis (PCA). Data were transformed to normality prior to statistical analyses using the procedures of Box and Cox. Differences in means were determined using 2-tailed *T*-tests or Mann–Whitney *U*-tests if normality was not achieved. The effects of frataxin gene on lipid profiles were assessed using multivariate analyses including correlations, cluster analyses and principal components analyses. Statistical operations were performed within Microsoft Excel. Multivariate and non-parametric statistics were performed using the Excel Add-In imDEV v1.4.2 (http://sourceforge.net/apps/mediawiki/imdev/index.php?title=Main_Page), which provides a graphical user interface to R-Programming language statistical packages (doi: 10.1093/bioinformatics/bts439).

SUPPLEMENTARY MATERIAL

Supplementary Material is available at *HMG* online.

Conflict of Interest statement. None declared.

FUNDING

The study was supported by NIH grants NS077777, EY012245 and AG025532 to G.A.C., and USDA-ARS Intramural Projects 5306-51530-019-00D and 1 U24 DK097154-01 to J.W.N. Funding to pay the Open Access publication charges for this article was provided by the NIH.

REFERENCES

- Campuzano, V., Montermini, L., Lutz, Y., Cova, L., Hindelang, C., Jiralerspong, S., Trottier, Y., Kish, S., Fauchoux, B., Trouillas, P. *et al.* (1997) Frataxin is reduced in Friedreich ataxia patients and is associated with mitochondrial membranes. *Hum. Mol. Genet.*, **6**, 10.
- Small, J.R., Thomas, P.K. and Schapira, A.H. (1993) Dorsal root ganglion proteins in Friedreich's ataxia. *Neurosci. Lett.*, **163**, 3.
- Ristow, M., Mulder, H., Pomplun, D., Schulz, T.J., Müller-Schmehl, K., Krause, A., Fex, M., Puccio, H., Müller, J., Isken, F. *et al.* (2003) Frataxin deficiency in pancreatic islets causes diabetes due to loss of β cell mass. *J. Clin. Invest.*, **112**, 527–534.
- Durr, A. and Brice, A. (2000) Clinical and genetic aspects of spinocerebellar degeneration. *Curr. Opin. Neurol.*, **13**, 7.
- Durr, A., Cossee, M., Agid, Y., Campuzano, V., Mignard, C., Penet, C., Mandel, J., Brice, A. and Koenig, M. (1996) Clinical and genetic abnormalities in patients with Friedreich's ataxia. *N. Engl. J. Med.*, **335**, 7.
- Campuzano, V., Montermini, L., Molto, D., Pianese, L., Cossee, M., Francesca Cavalcanti, T., Monros, E., Rodius, F., Duclos, F., Monticelli, A. *et al.* (1996) Friedreich's ataxia: autosomal recessive disease caused by an intronic GAA triplet repeat expansion. *Science*, **271**, 6.
- Cossee, M., Schmitt, M., Campuzano, V., Reutenauer, L., Moutou, J. and Koenig, M. (1997) Evolution of the Friedreich's ataxia trinucleotide repeat expansion: founder effect and premutations. *Proc. Natl Acad. Sci. USA*, **94**, 6.
- Wong, A., Yang, J., Cavadini, P., Gellera, C., Lonnerdal, B., Taroni, F. and Cortopassi, G. (1999) The Friedreich's ataxia mutation confers cellular sensitivity to oxidant stress which is rescued by chelators of iron and calcium and inhibitors of apoptosis. *Hum. Mol. Genet.*, **8**, 6.
- Chantrel-Groussard, K., Geromel, V., Puccio, H., Koenig, M., Munnich, A., Rötig, A. and Rustin, P. (2001) Disabled early recruitment of antioxidant defense in Friedreich's ataxia. *Hum. Mol. Genet.*, **10**, 8.
- Tan, G. (2003) Decreased expression of genes involved in sulfur amino acid metabolism in frataxin-deficient cells. *Hum. Mol. Genet.*, **12**, 1699–1711.
- Piemonte, F., Pastore, A., Tozzi, G., Tagliacozzi, D., Santorelli, F., Carrozzo, R., Casali, C., Damiano, M., Federici, G. and Bertini, E. (2001) Glutathione in blood of patients with Friedreich's ataxia. *Eur. J. Clin. Invest.*, **31**, 5.
- Schulz, J., Dehmer, T., Schols, L., Mende, H., Vorgerd, M., Burk, K., Matson, W., Dichgans, J., Beal, M. and Bogdanov, M.B. (2000) Oxidative stress in patients with Friedreich ataxia. *Neurology*, **55**, 3.
- Paupé, V., Dassa, E., Goncalves, S., Auchere, F., Lonn, M., Holmgren, A. and Rustin, P. (2009) Impaired nuclear Nrf2 translocation undermines the oxidative stress response in Friedreich ataxia. *PLoS One*, **4**, 11.
- Shan, Y., Schoenfeld, R.A., Hayashi, G., Napoli, E., Akiyama, T., Iodi Carstens, M., Carstens, E.E., Pook, M.A. and Cortopassi, G.A. (2013) Frataxin deficiency leads to defects in expression of antioxidants and Nrf2 expression in dorsal root ganglia of the Friedreich's ataxia YG8R mouse model. *Antioxid. Redox Signal.*, **19**, 1481–93.
- Al-Mahdawi, S., Pinto, R.M., Varshney, D., Lawrence, L., Lowrie, M.B., Hughes, S., Webster, Z., Blake, J., Cooper, J.M., King, R. *et al.* (2006) GAA repeat expansion mutation mouse models of Friedreich ataxia exhibit oxidative stress leading to progressive neuronal and cardiac pathology. *Genomics*, **88**, 580–590.
- Tian, X.Y., Wong, W.T., Leung, F.P., Zhang, Y., Wang, Y.X., Lee, H.K., Ng, C.F., Chen, Z.Y., Yao, X., Au, C.L. *et al.* (2012) Oxidative stress-dependent cyclooxygenase-2-derived prostaglandin f(2alpha) impairs endothelial function in renovascular hypertensive rats. *Antioxid. Redox Signal.*, **16**, 363–373.
- Smith, W., DeWitt, D. and Garavito, R.M. (2000) Cyclooxygenases: structural, cellular, and molecular biology. *Annu. Rev. Biochem.*, **69**, 145.
- Samuelsson, B., Goldyne, M., Granström, E., Hamberg, M., Hammarström, S. and Malmsten, C. (1978) Prostaglandins and thromboxanes. *Annu. Rev. Biochem.*, **47**, 33.
- Chen, Q., Miyaura, C., Higashi, S., Maurakami, M., Kudo, I., Saito, S., Hiraide, T., Shibasaki, Y. and Suda, T. (1997) Activation of cytosolic phospholipase A2 by platelet-derived growth factor is essential for cyclooxygenase-2-dependent prostaglandin E2 synthesis in mouse osteoblasts cultured with interleukin-1. *J. Biol. Chem.*, **272**, 5952–5958.
- Lu, C., Schoenfeld, R., Shan, Y., Tsai, H.J., Hammock, B. and Cortopassi, G. (2009) Frataxin deficiency induces Schwann cell inflammation and death. *Biochim. Biophys. Acta*, **1792**, 1052–1061.
- Wardlaw, S.A., Zhang, N. and Belinsky, S.A. (2002) Transcriptional regulation of basal cyclooxygenase-2 expression in murine lung tumor-derived cell lines by CCAAT/enhancer-binding protein and activating transcription factor/cAMP response element-binding protein. *Mol. Pharmacol.*, **62**, 326–333.
- Kang, Y.-J., Wingerd, B.A., Arakawa, T. and Smith, W.L. (2006) Cyclooxygenase-2 gene transcription in a macrophage model of inflammation. *J. Immunol.*, **177**, 8111–8122.
- Zhang, X., Zhang, J., Yang, X. and Han, X. (2007) Several transcription factors regulate COX-2 gene expression in pancreatic beta-cells. *Mol. Biol. Rep.*, **34**, 199–206.
- Shi, J., Wang, Q., Johansson, J.U., Liang, X., Woodling, N.S., Priyam, P., Loui, T.M., Merchant, M., Breyer, R.M., Montine, T.J. *et al.* (2012) Inflammatory prostaglandin E2 signaling in a mouse model of Alzheimer disease. *Ann. Neurol.*, **72**, 788–798.

25. Piro, J.R., Benjamin, D.I., Duerr, J.M., Pi, Y., Gonzales, C., Wood, K.M., Schwartz, J.W., Nomura, D.K. and Samad, T.A. (2012) A dysregulated endocannabinoid-eicosanoid network supports pathogenesis in a mouse model of Alzheimer's disease. *Cell Rep.*, **1**, 617–623.
26. Teismann, P., Tieu, K., Choi, D.K., Wu, D.C., Naini, A., Hunot, S., Vila, M., Jackson-Lewis, V. and Przedborski, S. (2003) Cyclooxygenase-2 is instrumental in Parkinson's disease neurodegeneration. *Proc. Natl Acad. Sci. USA*, **100**, 5473–5478.
27. Liang, X., Wang, Q., Shi, J., Lokteva, L., Breyer, R.M., Montine, T.J. and Andreasson, K. (2008) The prostaglandin E2 EP2 receptor accelerates disease progression and inflammation in a model of amyotrophic lateral sclerosis. *Ann. Neurol.*, **64**, 304–314.
28. Shin, J.H., Lee, Y.A., Lee, J.K., Lee, Y.B., Cho, W., Im, D.S., Lee, J.H., Yun, B.S., Springer, J.E. and Gwag, B.J. (2012) Concurrent blockade of free radical and microsomal prostaglandin E synthase-1-mediated PGE2 production improves safety and efficacy in a mouse model of amyotrophic lateral sclerosis. *J. Neurochem.*, **122**, 952–961.
29. Miranda, C.J., Santos, M.M., Ohshima, K., Smith, J., Li, L., Bunting, M., Cosse, M., Koenig, M., Sequeiros, J., Kaplan, J. *et al.* (2002) Frataxin knockin mouse. *FEBS Lett.*, **512**, 291–297.
30. Capdevila, J.H., Falck, J.R. and Estabrook, R.W. (1992) Cytochrome P450 and the arachidonate cascade. *FASEB J.*, **6**, 731–736.
31. O'Flaherty, J.T., Kuroki, M., Nixon, A.B., Wijkander, J., Yee, E., Lee, S.L., Smitherman, P.K., Wykle, R.L. and Daniel, L.W. (1996) 5-Oxo-eicosanoids and hematopoietic cytokines cooperate in stimulating neutrophil function and the mitogen-activated protein kinase pathway. *J. Biol. Chem.*, **271**, 17821–17828.
32. Praticò, D., Zhukareva, V., Yao, Y., Uryu, K., Funk, C.D., Lawson, J.A., Trojanowski, J.Q. and Lee, V.M.Y. (2004) 12/15-Lipoxygenase is increased in Alzheimer's disease: possible involvement in brain oxidative stress. *Am. J. Pathol.*, **164**, 1655–1662.
33. Lin, L.L., Lin, A.Y. and Knopf, J.L. (1992) Cytosolic phospholipase A2 is coupled to hormonally regulated release of arachidonic acid. *Proc. Natl Acad. Sci. USA*, **89**, 6147–6151.
34. Dewitt, D.L. and Meade, E.A. (1993) Serum and glucocorticoid regulation of gene transcription and expression of the prostaglandin H synthase-1 and prostaglandin H synthase-2 isozymes. *Arch. Biochem. Biophys.*, **306**, 94–102.
35. Qin, Y., Hua, M., Duan, Y., Gao, Y., Shao, X., Wang, H., Tao, T., Shen, A. and Cheng, C. (2012) TNF-alpha expression in Schwann cells is induced by LPS and NF-kappaB-dependent pathways. *Neurochem. Res.*, **37**, 722–731.
36. Koeppen, A.H. (2011) Friedreich's ataxia: pathology, pathogenesis, and molecular genetics. *J. Neurol. Sci.*, **303**, 1–12.
37. Harding, A. (1981) Friedreich's ataxia: a clinical and genetic study of 90 families with an analysis of early diagnostic criteria and intrafamilial clustering of clinical features. *Brain*, **104**, 589–620.
38. Al-Mahdawi, S., Pinto, R.M., Ismail, O., Varshney, D., Lymperi, S., Sandi, C., Trabzuni, D. and Pook, M. (2008) The Friedreich ataxia GAA repeat expansion mutation induces comparable epigenetic changes in human and transgenic mouse brain and heart tissues. *Hum. Mol. Genet.*, **17**, 735–746.
39. Sanchez-Mejia, R.O., Newman, J.W., Toh, S., Yu, G.-Q., Zhou, Y., Halabisky, B., Cisse, M., Seearce-Levie, K., Cheng, I.H., Gan, L. *et al.* (2008) Phospholipase A2 reduction ameliorates cognitive deficits in a mouse model of Alzheimer's disease. *Nat. Neurosci.*, **11**, 1311–1318.
40. Xi, S., Pham, H. and Ziboh, W.A. (2000) 15-hydroxyeicosatrienoic acid (15-HETE) suppresses epidermal hyperproliferation via the modulation of nuclear transcription factor (AP-1) and apoptosis. *Arch. Dermatol. Res.*, **292**, 397–403.
41. Node, K., Huo, Y., Ruan, X., Yang, B., Spiecker, M., Ley, K., Zeldin, D.C. and Liao, J.K. (1999) Anti-inflammatory properties of cytochrome P450 epoxygenase-derived eicosanoids. *Science*, **285**, 1276–1279.
42. Capdevila, J., Chacos, N., Werrington, J., Prough, R.A. and Estabrook, R.W. (1981) Liver microsomal cytochrome P-450 and the oxidative metabolism of arachidonic acid. *Proc. Natl Acad. Sci. USA*, **78**, 5362–5366.
43. Feng, L., Xia, Y., Garcia, G.E., Hwang, D. and Wilson, C.B. (1995) Involvement of reactive oxygen intermediates in cyclooxygenase-2 expression induced by interleukin-1, tumor necrosis factor-alpha, and lipopolysaccharide. *J. Clin. Invest.*, **95**, 1669–1675.
44. Block, M.L. and Hong, J.S. (2005) Microglia and inflammation-mediated neurodegeneration: multiple triggers with a common mechanism. *Prog. Neurobiol.*, **76**, 77–98.
45. Yan, X.D., Kumar, B., Nahreini, P., Hanson, A.J., Prasad, J.E. and Prasad, K.N. (2005) Prostaglandin-induced neurodegeneration is associated with increased levels of oxidative markers and reduced by a mixture of antioxidants. *J. Neurosci. Res.*, **81**, 85–90.
46. Strokin, M., Sergeeva, M. and Reiser, G. (2007) Prostaglandin synthesis in rat brain astrocytes is under the control of the n-3 docosahexaenoic acid, released by group VIB calcium-independent phospholipase A2. *J. Neurochem.*, **102**, 1771–1782.
47. Li, X., Song, L. and Jope, R.S. (1996) Cholinergic stimulation of AP-1 and NF-kB transcription factors is differentially sensitive to oxidative stress in SH-SY5Y neuroblastoma: relationship to phosphoinositide hydrolysis. *J. Neurosci.*, **16**, 5914–5922.
48. Rojo, A.I., Innamorato, N.G., Martin-Moreno, A.M., De Ceballos, M.L., Yamamoto, M. and Cuadrado, A. (2010) Nrf2 regulates microglial dynamics and neuroinflammation in experimental Parkinson's disease. *Glia*, **58**, 588–598.
49. Michael, S., Petrocine, S.V., Qian, J., Lamarche, J.B., Knutson, M.D., Garrick, M.D. and Koeppen, A.H. (2006) Iron and iron-responsive proteins in the cardiomyopathy of Friedreich's ataxia. *Cerebellum*, **5**, 257–267.
50. Castaldo, I., Pinelli, M., Monticelli, A., Acquaviva, F., Giacchetti, M., Filla, A., Sacchetti, S., Keller, S., Avvedimento, V.E., Chiariotti, L. *et al.* (2008) DNA methylation in intron 1 of the frataxin gene is related to GAA repeat length and age of onset in Friedreich ataxia patients. *J. Med. Genet.*, **45**, 808–812.
51. Wong, J.Y.Y., De Vivo, I., Lin, X., Fang, S.C. and Christiani, D.C. (2014) The relationship between inflammatory biomarkers and telomere length in an occupational prospective cohort study. *PLoS One*, **9**, e87348.
52. Masi, S., Salpea, K.D., Li, K., Parkar, M., Nibali, L., Donos, N., Patel, K., Taddei, S., Deanfield, J.E., D'Aiuto, F. *et al.* (2011) Oxidative stress, chronic inflammation, and telomere length in patients with periodontitis. *Free Radic. Biol. Med.*, **50**, 730–735.